Eddy diffusion

December 7, 2000

1 Introduction

Perhaps you have heard that turbulence is the most difficult problem in fluid mechanics and, according to some, the greatest unsolved problem in physics. One indication of the difficulty is that it is impossible to give a satisfactory definition of a "turbulent flow". But everyone agrees that one property of turbulence is greatly enhanced transport of passive contaminants. For example, relying only on molecular agitation, a dissolved sugar molecule takes years to diffuse across a coffee cup, and on that time-scale the coffee will surely evaporate. With a spoon the coffee drinker can create eddies that transport dissolved sugar throughout the cup in less than one second. This is an example of *eddy diffusivity*.

Fluid mechanics textbooks often often justify eddy diffusivity by appealing to an analogy between turbulent eddies and molecular diffusion — perhaps this notion originates with G.I. Taylor's 1915 paper entitled "Eddy motion in the atmosphere"? In any event, the molecular analogy, supplemented with some hand-waving, leads to the notion of an eddy diffusivity and for many scientists this is the end of the turbulence problem.

Our goal in this lecture is to explain very explicitly the assumptions behind Taylor's "proof by analogy" and to illustrate the interesting points at which the analogy fails. We will pursue this program by working with some very simple model flows for which analytic results, such as expressions for the eddy diffusivity, are available. As you will soon see, these model flows do not greatly resemble turbulence, but then neither does molecular motion! Our excuse is that soluble examples are always diverting and educational.

2 The renovating wave model

A recipe for constructing soluble models

The main problem in analyzing transport is solving the differential equations which describe the motion of particles in even very simple flows. However there is a class of flows for which this task is trivial. These are steady and unidirectional flows, such as $u = \sin y$. A particle which starts at (a, b) at $t = 0$ finds itself at $(a + \tau \sin b,\, b)$ at $t = \tau$. This is dull, but it becomes more interesting if at intervals of τ we "renovate" the flow by randomly picking a new direction along which the velocity acts. In this way we can construct a sequence of iterated random maps and calculate diffusivities, and other statistical properties, by averaging the exact solution. I learned of this trick from the literature on dynamo theory. The book *Stretch, Twist, Fold: the Fast Dynamo* is highly recommended for students interested in all aspects of stirring and mixing. .

2.1 The renovating wave (RW) model

As a particular example we now formulate the *renovating wave* (RW) model. We divide the time axis into intervals

$$I_n \equiv \{t : (n-1)\tau < t < n\tau\}\,, \tag{1}$$

and in each interval we apply a velocity, $\boldsymbol{u} = (-\psi_y, \psi_x)$, derived from the streamfunction

$$\psi_n(x, y, t) = k^{-1} U \cos[k \cos\theta_n\, x + k \sin\theta_n\, y + \varphi_n]\,, \tag{2}$$

where θ_n and φ_n are independent random variables uniformly distributed in the interval $[-\pi, \pi]$. Thus in each I_n there is a steady, unidirectional velocity with sinusoidal profile (a single wave). There is sudden and complete loss of all information about the past velocity at $t = n\tau$ because at these instants we "renovate" the velocity by picking new random angles θ and φ. (This means that the velocity correlation function, $\mathcal{C}(t)$, is zero if $t > \tau$.)

The renovating wave model can be nondimensionalized by using k^{-1} as a unit of length and and $1/(Uk)$ as a unit of time. With this choice, the model contains a single dimensionless parameter, $\tau_* \equiv \tau k U$, which is a measure of

the persistence of the motion. Much of the literature on random advection-diffusion uses model velocity fields which are δ-correlated in time. We can recover this limit as a special case by taking $\tau_* \to 0$.

Using dimensionless variables, a particle which is at $\boldsymbol{x}_n = (x_n, y_n)$ at $t_n = n\tau_*$ moves to $\boldsymbol{x}_{n+1}$ at $t = (n+1)\tau_*$ where

$$(x_{n+1}, y_{n+1}) = (x_n, y_n) + \tau_* \sin\left(c_n x + s_n y + \varphi_n\right)(s_n, -c_n)\,. \tag{3}$$

with $s_n \equiv \sin\theta_n$ and $c_n \equiv \cos\theta_n$. Thus motion in the renovating wave problem is equivalent to an iterated sequence of random maps.

2.2 The single–particle diffusivity

It is very easy to calculate the diffusivity in the RW model (and much more difficult to interpret the answer). The average of a function of the two random angles θ and φ (suppress the subscript n) is defined by

$$\langle f \rangle = \oint \frac{\mathrm{d}\varphi}{2\pi} \oint \frac{\mathrm{d}\theta}{2\pi} f(\theta, \varphi). \tag{4}$$

Therefore, using (3),

$$\left\langle (x_{n+1} - x_n)^2 \right\rangle = \frac{\tau_*^2}{4}\,. \tag{5}$$

The computation is trivial if the integral over φ is evaluated first.

In (5), following our previous discussion based on Einstein's derivation of the diffusion equation, we are computing the statistics of dispersion along the x-axis. Because the renovating wave model is isotropic, dispersion in the y-direction is identical to that in the x-direction.

Because all of the waves are independent and identically distributed it follows that after n renovation cycles

$$\left\langle (x_n - x_0)^2 \right\rangle = n\frac{\tau_*^2}{4}. \tag{6}$$

But $t = n\tau_*$, and $\left\langle (x_n - x_0)^2 \right\rangle = 2Dt$, so that using dimensionless variables the diffusivity is

$$D = \frac{\tau_*}{8}. \tag{7}$$

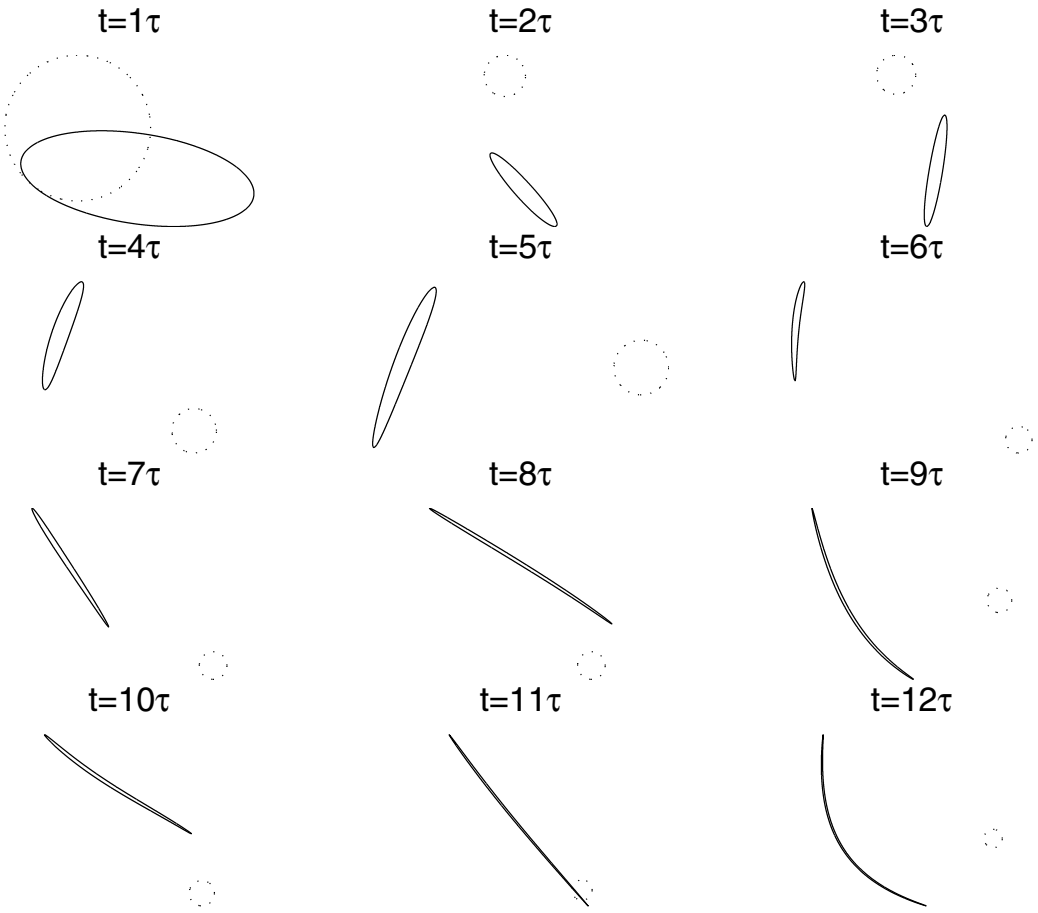

Figure 1: Stretching of a small spot, $r \ll 1$ where r is the initial radius of the spot, by a succession of random sinusoidal flows. The dotted circle is the initial spot.

Sometimes D is referred to as the single-particle diffusivity. "Single-particle" emphasizes that D strictly applies only to the RMS displacement of a particle from its initial position; D contains no information concerning the deformation of a patch of tracer, nor of any other quantity involving correlated motion. Thus, using dimensional variables, the diffusivity in (7) is $D = U^2\tau/8$, which is independent of k. Because D is independent of the scale of the wave, even a spatially uniform, but random-in-time velocity (the case $k = 0$), has a single-particle diffusivity.

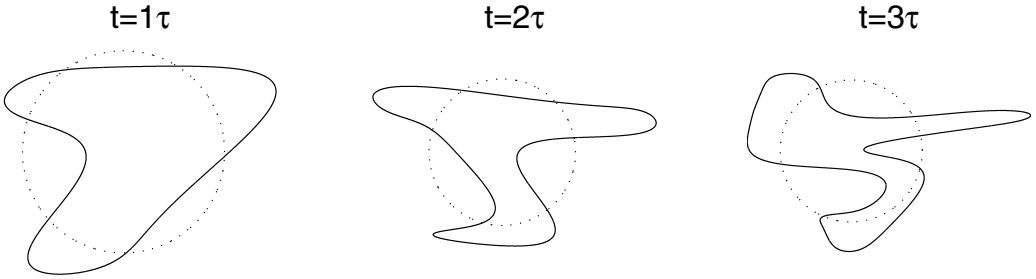

Figure 2: Stretching of a blob with $r = 1$, where r is the initial radius. The dotted circle is the initial patch.

2.3 Deformation of variously sized blobs

To emphasize the importance of understanding more than single-particle diffusivities we take a digression and illustrate how the deformation of an initially circular blob of fluid depends on the blob radius r. (Recall that we have used k^{-1} as unit of length; in terms of dimensional variables the relevant nondimensional parameter is kr.)

If the initial blob is much smaller than the wavelength of the velocity then on the scale of the blob the velocity profile is a linear function of the coordinates. Because of this simplicity, the first few iterations deform the circular blob into an ellipse which must have the same area as the initial circle. We will see in the next lecture that the major axis of the ellipse grows exponentially while the minor axis shrinks so that the area is fixed. Once the dimensions of the ellipse are comparable to the wavenumber of the flow, more complicated deformations occur. Ultimately the blob will be stretched into a folded filament as in figure 1.

The blob has the same scale as the velocity field if $r \sim 1$. Because there is no *scale separation* there is no easy description of the action of the flow on the blob, see figure 2.

If $r \gg 1$ then we are in the "eddy diffusivity" limit in which the scale of the velocity field is much smaller than the scale of the tracer. This case is shown in figure 3. The action of the waves perturbs the edge of the blob, making it look "fuzzy". In fact, the area is preserved, but the circumference of the blob grows exponentially. We will be discussing this type of problem for the remainder of this lecture.

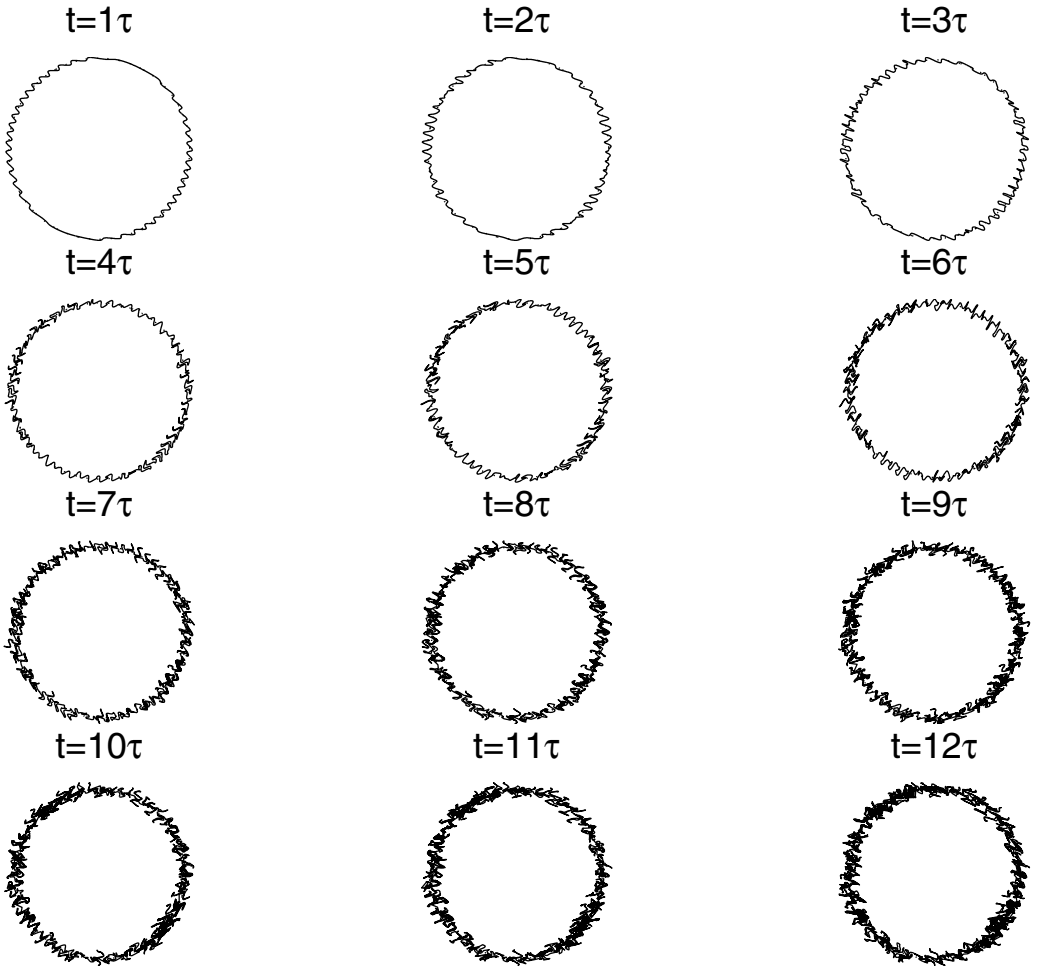

Figure 3: Stretching of a big blob $r \gg 1$, where r is the initial radius of the blob. The dotted circle representing the initial patch may not be visible beneath the wiggly boundary of the blob.

2.4 The Lagrangian correlation function

In (7) we gave the diffusivity of particles moving in an ensemble of renovating waves. How do we obtain the Lagrangian velocity autocorrelation function and verify Taylor's formula that

$$D = \int_0^\infty \mathcal{C}(t)\,\mathrm{d}t\,? \tag{8}$$

Considering this question, we encounter an annoying technical difficulty: our derivation of (8) assumes that the velocity statistics are stationary. But the renovating wave ensemble, as we defined it back in (1) and (2), is not a stationary stochastic process. This is because with our original definition all members of the ensemble renovate at the same instants $t = \tau$, $t = 2\tau$ etcetera. In order to obtain a stationary process we should initiate different realizations at uniformly distributed points during the renovation cycle. Thus, for realization number j, we pick a random time $\tau^{(j)}$ which is uniformly distributed in the interval $[0, \tau]$ and renovate first at $t = \tau^{(j)}$ and then subsequently at $t = \tau^{(j)} + \tau$, $t = \tau^{(j)} + 2\tau$ etcetera. With this new and improved formulation of the RW model the Lagrangian correlation function of $u(t)$ is a "triangular" function:

$$\mathcal{C}(t) = \frac{U^2}{4}\left(1 - \frac{t}{\tau}\right) H(\tau - t)\,, \tag{9}$$

where H is the step function and U is the velocity in (2). The area of under this correlation function is $D = U^2\tau/8$.

3 The eddy diffusion equation

3.1 The ensemble averaged Green's function

Now that we have obtained the RW diffusivity in (7) we turn to the derivation of the eddy diffusion equation. For each realization we introduce the Green's function which is

$$G_t + \boldsymbol{u}\cdot\nabla G = 0, \quad \text{with} \quad G(\boldsymbol{x}, \boldsymbol{x}_0, 0) = \delta(\boldsymbol{x} - \boldsymbol{x}_0). \tag{10}$$

The solution of the problem above is

$$G(\boldsymbol{x}, \boldsymbol{x}_0, t) = \delta(\boldsymbol{x}_t - \boldsymbol{x}_0)\,, \tag{11}$$

where $\boldsymbol{x}_t$ is the position at time t (in a particular realization of $\boldsymbol{u}$) of the particle which started at $\boldsymbol{x}_0$.

The ensemble averaged Green's function is

$$g(r, t) = \langle G(\boldsymbol{x}, \boldsymbol{x}_0, t)\rangle\,, \qquad r \equiv |\boldsymbol{x} - \boldsymbol{x}_0|\,, \tag{12}$$

where we have assumed that the random velocity is isotropic, homogeneous and stationary so that g can depend only on the distance r and the elapsed time t.

Possessing $g(r,t)$, we can then represent the ensemble-averaged solution of the initial value problem

$$c_t + \boldsymbol{u}\cdot\nabla c = 0, \qquad c(\boldsymbol{x},0) = c_0(\boldsymbol{x})\,, \tag{13}$$

as the convolution

$$\langle c\rangle(\boldsymbol{x},t) = \int c_0(\boldsymbol{x}-\boldsymbol{x}')g(|\boldsymbol{x}'|,t)\,\mathrm{d}\boldsymbol{x}'\,. \tag{14}$$

(We are assuming that the initial condition c_0 is the same for all realizations.)

At this point, the analogy between (14) and the master equation of lecture 1 is obvious. With the master equation in mind, we can anticipate that a variant of Einstein's derivation of the diffusion equation can be applied to (14). Rather than develop a general derivation we prefer to use the renovating wave model as a concrete illustration of how one can obtain g, and then pass from the integral equation in (14) to an approximate diffusion equation.

3.2 The averaged Green's function of the RW model

There are at least two ways of obtaining $g(r)$ in (12) for the RW model: the hard, straightforward way (see the appendix) and the easy, devious way. Let us be devious.

We begin by calculating the probability density function (PDF) of displacements in a single pulse of the RW model. Because the ensemble of velocities is isotropic and homogeneous there is no harm in supposing that the particle is at the origin and the x-axis is aligned with the direction of the velocity. That is, put $(x_n, y_n) = (0,0)$ and $\theta_n = \pi/2$ in (3). Thus, the displacement r produced by a single pulse is

$$x_{n+1} - x_n = \tau_* \sin\varphi_n, \quad \text{and} \quad r = |x_{n+1} - x_n|. \tag{15}$$

The PDF of the random variable r can be obtained from the PDF of φ, that is $P(\varphi) = 1/2\pi$, using the rule for transforming probabilities:

$$P(r) = \sum P(\varphi)\Big|\frac{\mathrm{d}\varphi}{\mathrm{d}r}\Big|, \quad \Rightarrow \quad P(r) = \frac{2}{\pi}\frac{H(\tau_* - r)}{\sqrt{\tau_*^2 - r^2}}\,. \tag{16}$$

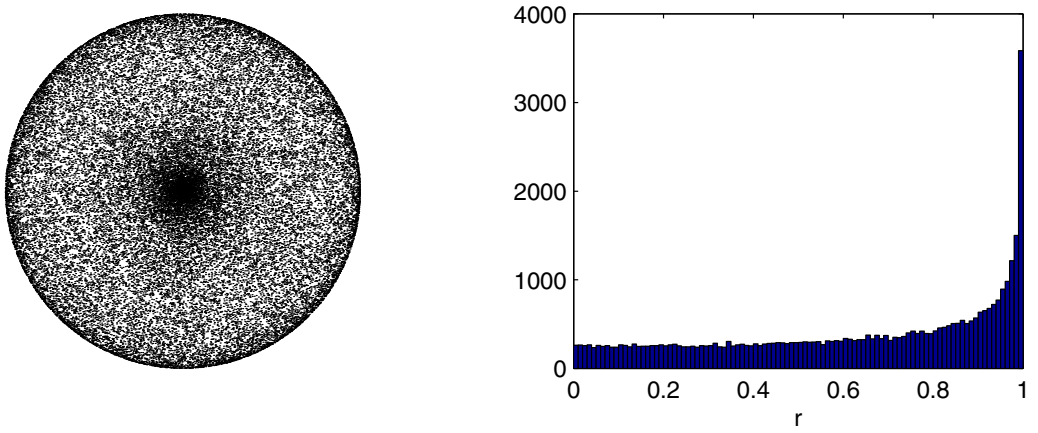

Figure 4: Displacements of $40,000$ particles in independent realizations of the the RW model. The left panel shows the final position of particles which all start at the center of the the circle after one pulse of the wave. The density of points corresponds to $g(r)$ in (17). The histogram on the right shows the number of particles at a distance r from the center; this is the function $P(r)$ in (16).

In (16) $H(\tau_* - r)$ is a Heaviside step function which ensures that there are no displacements greater than τ_*. (The sum in (16) is because there are four values of φ corresponding to a single value of r.)

The averaged Green's function is now given by

$$g(r) = \frac{P(r)}{2\pi r}\,, \qquad \Rightarrow \qquad g(r) = \frac{1}{\pi^2}\frac{H(\tau_* - r)}{r\sqrt{\tau_*^2 - r^2}}\,. \tag{17}$$

The geometric factor $2\pi r$ is included because $g(r)$ is a concentration. That is, $P(r)\mathrm{d}r$ the expected number of particles which fall into the differential annulus between r and $r + \mathrm{d}r$ and $g(r)$ is the expected number of particles *per area* in this same annulus; see figure 4.

Now that we have the averaged Green's function of a single pulse we can obtain the evolution the ensemble averaged concentration, $\langle c\rangle$, over many pulses. Because each pulse is independent of the preceeding pulses we have

$$\langle c\rangle\,(\boldsymbol{x}, (n+1)\,\tau_*) = \int\langle c\rangle(\boldsymbol{x} - \boldsymbol{x}', n\tau_*)g(|\boldsymbol{x}'|)\,\mathrm{d}\boldsymbol{x}'\,. \tag{18}$$

The master equation above, with $g(r)$ in (17), is an exact description of the evolution of $\langle c\rangle$ under advection by the RW model.

3.3 The diffusion equation

With the master equation (18) in hand, we can use Einstein's approximations to obtain the diffusion equation. Using the dimensionless variables of the renovating wave model, we have

$$\langle c\rangle_t \approx \frac{\tau_*}{8}\nabla^2\langle c\rangle\,. \tag{19}$$

We leave this as a homework exercise and instead we take a different route to (19).

Because the Fourier transform of a convolution is the product of the Fourier transforms, we can simplify (18) by transforming. The Fourier transform of $f(\boldsymbol{x})$ is defined here[1] as

$$\tilde{f}(\mathbf{k}) = \int e^{-\mathrm{i}\mathbf{k}\cdot\boldsymbol{x}} f(\boldsymbol{x})\,\mathrm{d}x\,, \qquad f(\boldsymbol{x}) = \frac{1}{2\pi}\int e^{\mathrm{i}\mathbf{k}\cdot\boldsymbol{x}}\tilde{f}(\mathbf{k})\,\mathrm{d}k\,. \tag{20}$$

Applying the transform to (18) we obtain

$$\widetilde{\langle c\rangle}(\mathbf{k}, n\tau_*) = \tilde{g}(k)^n\tilde{c}_0(\mathbf{k})\,, \qquad k \equiv |\mathbf{k}|\,. \tag{21}$$

With a good table of integrals one can discover that the Fourier transform of the averaged Green's function, $g(r)$ in (17), is

$$\tilde{g}(k) = J_0^2(k\tau_*/2)\,, \tag{22}$$

where J_0 is the Bessel function.

The diffusion equation describes the evolution of large spatial scales, which is the same as small wavenumbers. This means that we simplify (21) by taking $k\tau_*/2 \ll 1$ and using the approximation $J_0(k\tau_*/2) \approx 1-(k^2\tau_*^2/16)$ to write

$$\widetilde{\langle c\rangle}(\mathbf{k}, n\tau_*) \approx \exp\left\{n\ln\left[1-(k^2\tau_*^2/8)\right]\right\}\tilde{c}_0(\mathbf{k})\,. \tag{23}$$

But now, since $n = t/\tau_*$ and $\ln[1-(k^2\tau_*^2/8)] \approx -k^2\tau_*^2/8$, we have

$$\widetilde{\langle c\rangle}(\mathbf{k}, t) = e^{-Dk^2t}\tilde{c}_0(\mathbf{k}) \tag{24}$$

where, as in (19), $D = \tau_*/8$. Equation (24) is the equivalent to the decay of Fourier components given by (19).

This derivation based on Fourier analysis explicitly recognizes that the diffusion approximation is valid only for wavenumbers which satisfy $k\tau_*/2 \ll 1$. This is a precise statement of the scale separation assumption which underlies Einstein's approach.

[1] By denoting the wavenumber with k we are recycing notation used in (2).

4 Ensemble averages and single realizations

In hydrodynamic dispersion, particles which begin at neighbouring points have similar histories in any single realization. Marbled endpapers in old books were produced by floating coloured inks on water, stirring the surface, and then capturing the swirls by carefully lowering a sheet of paper onto the inky film [3]. This technique, probably originating in Persia in the 1400s, presses hydrodynamic correlations into the service of art. Fortunately for printers, and distressingly for statisticians, a single realization does not resemble the blurry diffusion equation.

4.1 Eddy diffusion of a front

Figure 5 shows a single realization of the evolution of a "front" under the RW advection process. The front is the sharp border which separates white from dark; initially this line coincides with the y-axis. We suppose that the concentration is $c = -1$ for $x < 0$ and $c = +1$ for $x > 0$. Successive pulses of the renovating wave produce an increasingly folded front and the $c = -1$ fluid invades the region $x > 0$ in long thin tendrils. The central question is:

How well is the process in figure 5 described by the diffusion equation?

We know that given many realizations of this process, the long-time ensemble average of these realizations will follow the diffusion equation $\langle c \rangle_t = D\langle c \rangle_{xx}$, with the initial conditions $c(x, 0) = \pm 1$. The solution of this problem is

$$\langle c \rangle = \mathrm{erf}\eta\,, \qquad \text{where} \qquad \eta = \frac{x}{2\sqrt{Dt}}\,. \tag{25}$$

Figure 6 shows this smooth erf solution which, of course, looks nothing like figure 5. If the dark fluid in figure 5 contained radioactive contaminant, and we wanted to estimate the *maximum* exposure of at some value of $x > 0$, then the erf solution in (25) is not useful.

On the other hand, diffusivities are useful if we want to know how many particles are at such-and-such a distance from their initial location. Thus, figure 7 shows a histogram of the positions of 10,000 particles which all start on the line $x = 0$ (the initial front). The Gaussian curve in figure 7 is

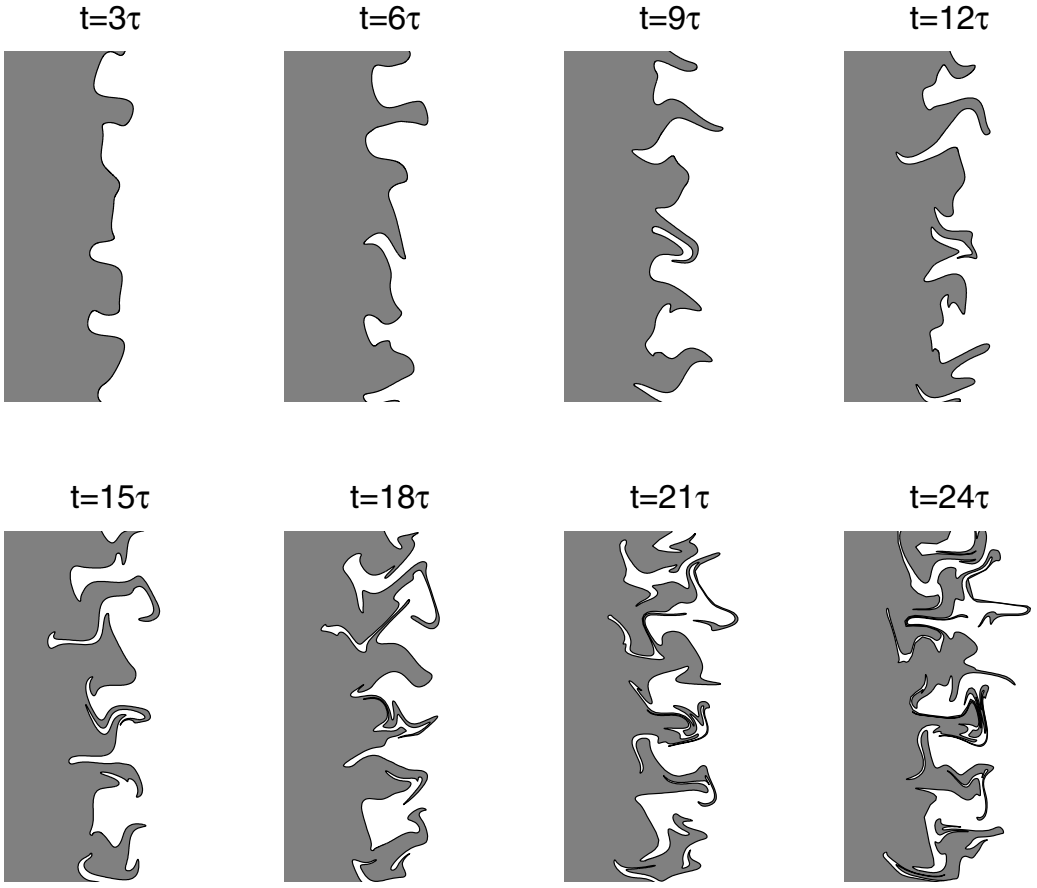

Figure 5: Evolution of a front under the advection by the RW model. The front initially coincides with the y-axis.

the corresponding prediction for the PDF of positions which is obtained by solving (19) with the initial condition $\langle c \rangle = \delta(x)$:

$$c(x,t) = \frac{1}{\sqrt{4\pi D t}} \exp\left[-\frac{x^2}{4Dt}\right], \qquad D = \frac{\tau_*}{8}. \tag{26}$$

The histograms converge slowly to this Gaussian prediction. This asymptotic success shows that the diffusion equations correctly predicts the dispersion of particles when $t \gg \tau_*$.

An amusing aspect of the simple problem in figure 5 is that we can easily calculate the RMS fluctuations of c around the ensemble average concentra-

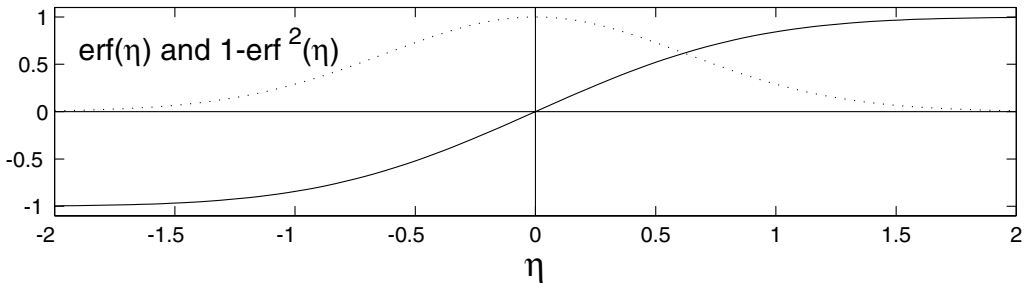

Figure 6: Evolution of the ensenble-averaged concentration c and its variance during the evolution of the front underthe RRW model. Note how most of the variance is localised around $x = 0$.

tion in (25). Because $c = \pm 1$ we have $\langle c^2 \rangle = 1$. Therefore, defining the fluctuation as

$$c' = c - \langle c \rangle \,, \tag{27}$$

we have

$$\langle c'^2 \rangle = \langle c^2 \rangle - \langle c \rangle^2 = 1 - \mathrm{erf}^2(\eta) \,. \tag{28}$$

The variance $\langle c'^2 \rangle$ is also indicated in figure 6.

4.2 Coarse grained averages and spatial filters

The process in figure 5 is translationally invariant in the y-direction and so using only a single realization we can calculate a spatially averaged concentration

$$\bar{c}(x,t) \equiv \lim_{L\to\infty} \frac{1}{2L} \int_{-L}^{L} c(x,y,t) \mathrm{d}y \,. \tag{29}$$

The evolution of $\bar{c}$ will be asymptotically described by the diffusion equation.

In a general case, in which there is no statistical symmetry along a particular direction, one can take a single realization and define a coarse-grained or low-pass filtered concentration by:

$$\hat{c}(\boldsymbol{x},t) \equiv \int K(\boldsymbol{x}-\boldsymbol{x}') c(\boldsymbol{x}',t) \, \mathrm{d}^2\boldsymbol{x}' \,; \qquad K(|\boldsymbol{x}|) \text{is a filter.} \tag{30}$$

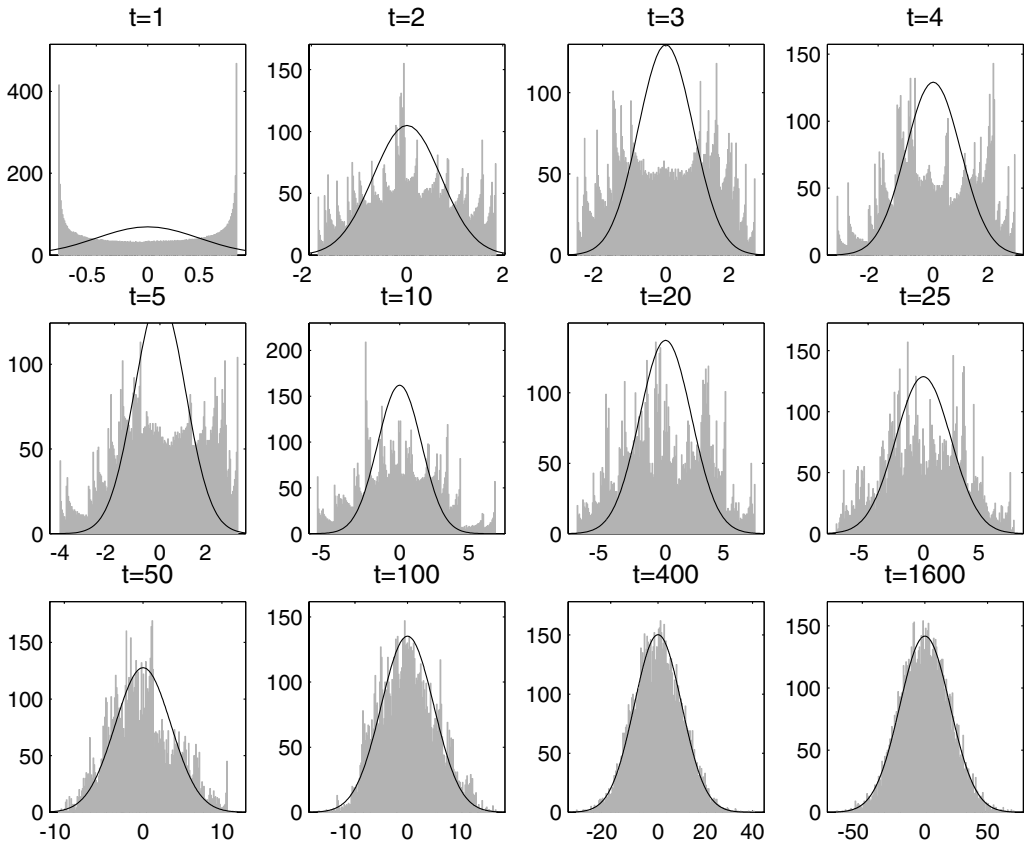

Figure 7: At $t = 0$ the front in figure 5 is tagged by placing 10000 particles along the y-axis. The historgram above shows the subsequent x-locations of these marker particles as the front is distorted by the RW model with $\tau_* = 1$. The Gaussian curve is given by (26).

The hope is that scale separation between the width of the erf and the swirls will ensure that $\hat{c} \approx \langle c \rangle$. Thus the kernel of the filter, K in (30), might be a Gaussian with a width which is at once much smaller than the thickness of the erf transition zone and much greater than an individual swirl in figure 5.

Scale separation is essential here because the filtering operation defined by the convolution in (30) is not strictly an "average". Some of the properties we take for granted when we use averages are

$$\langle c' \rangle = 0\,, \qquad \langle\langle c \rangle\rangle = \langle c \rangle\,, \qquad \langle\langle a \rangle\langle b \rangle\rangle = \langle a \rangle\langle b \rangle\,. \tag{31}$$

For the ensemble average, as indicated in (31), everything works.

For a filter, such as $\hat{}$ in (30), we can define the fluctuation concentration c'' in analogy with (27):

$$c'' \equiv c - \hat{c}\,. \tag{32}$$

But then $\widehat{c''} \neq 0$ and none of the other desiderata in (31) follow. In other words, spatial filtering instead of the ensemble averaging introduces a host of extra assumptions which should be carefully assessed (but almost never are).

4.3 A digression: Brownian bugs

I have hinted darkly at problems associated with spatial filters. These issues are largely ignored by optimistic scientists. The hope is that scale separation justifies the application of diffusive closures to the coarse-grained version of a single realization. Perhaps a justification of this optimistic approach is that the alternative seems so repellant. Nonetheless, it is important to realize that interpreting coarse-grained distributions as ensemble averages involves a nontrivial assumption. The best way of exposing this assumption is to exhibit a problem in which spatial filters and ensemble averages are very different. Accordingly, as a model of biological processes, we consider random walkers which both die and reproduce. We refer to these biological walkers as Brownian bugs.

The model is formulated by first placing $N \gg 1$ Brownian bugs randomly in the unit square; the boundary conditions are periodic in both directions. Each cycle of the simulation begins with a random walk step in which bug k, located at $\boldsymbol{x}_k = (x_k, y_k)$, is displaced to a new position

$$(x_k', y_k') = \mathrm{mod}\left[(x_k, y_k) + (\delta x_k, \delta y_k); 1\right]. \tag{33}$$

In (33), δx_k and δy_k are Gaussian random variables and the "mod" is to enforce the periodic boundary conditions and keep each bug in the unit square. After this random walk step, the second part of the cycle is a "coin toss" which results in either death (heads) or division (tails). When a lucky bug divides, the offspring is placed at the same position as the parent. This cycle of random displacement and random birth/death is repeated many times in order to simulate many generations of reproduction, death and dispersion.

The simulation shown in figure 8 was implemented in MATLAB using these rules. The striking result is that the density of bugs spontaneously

develops large-scale clumps and voids. Figure 8 seems to show an inverse cascade of patch sizes: patches emerge on small scales in panel (b) and then, after more cycles, panels (c) and (d) show that the patches have expanded in scale. To quantify this impression, we have computed one-dimensional concentration spectra which show that an increasingly red spectrum develops.

A seemingly innocuous ingredient of the brownian-bug model is that deaths can occur anywhere, but births are always adjacent to a living bug. This asymmetry between birth and death is crucial for the spontaneous development of the voids and patches evident in figure 8: if one simulates birth by randomly placing the new bugs in the unit square then no patches form. This subtle point shows that making the births coincide with living bugs — surely a realistic feature of the model — introduces *pair* correlations. From another perspective, one can view the voids in figure 8 as the result of random extinctions which create voids. The step length of the random walk in figure 8 is such that diffusion is not strong enough to fill in the voids created by extinction.

The ensemble average of the Brownian bug process is described by

$$\langle c\rangle_t = D\nabla^2\langle c\rangle + (\lambda-\mu)\langle c\rangle\,. \tag{34}$$

where λ is the birthrate and μ the deathrate. However if the coin-toss is fair then births and deaths are equiprobable and consequently $\lambda = \mu$. In this case the solution of (34) which satisfies the initial condition is

$$\lambda = \mu\,, \qquad \Rightarrow \qquad \langle c\rangle = 1/N\,. \tag{35}$$

The uniform density above is the correct answer for the *ensemble* average concentration: the location of the voids and patches in figure 8 are accidently determined by the MATLAB random number generator. If we ensemble average many such patterns then the patches and voids must disappear because the process is spatially homogeneous.

On the other hand, the spatial average of a single realization, such as that in figure 8, will still show concentration patches[2]. Thus, in this Brownian bug example, $\hat{c} \neq \langle c\rangle$. Indeed, the patches are surely an important feature of the "real" answer. The correct but useless result in (35) exposes a failure of ensemble averaging. What do we make of this example? Are biological

[2]If the width of the kernel, K in (30), is larger than the dimension of the patches then filtering will remove the patches. However, since the patches expand in scale, eventually they will become so large that they survive the blurring power of the filter.

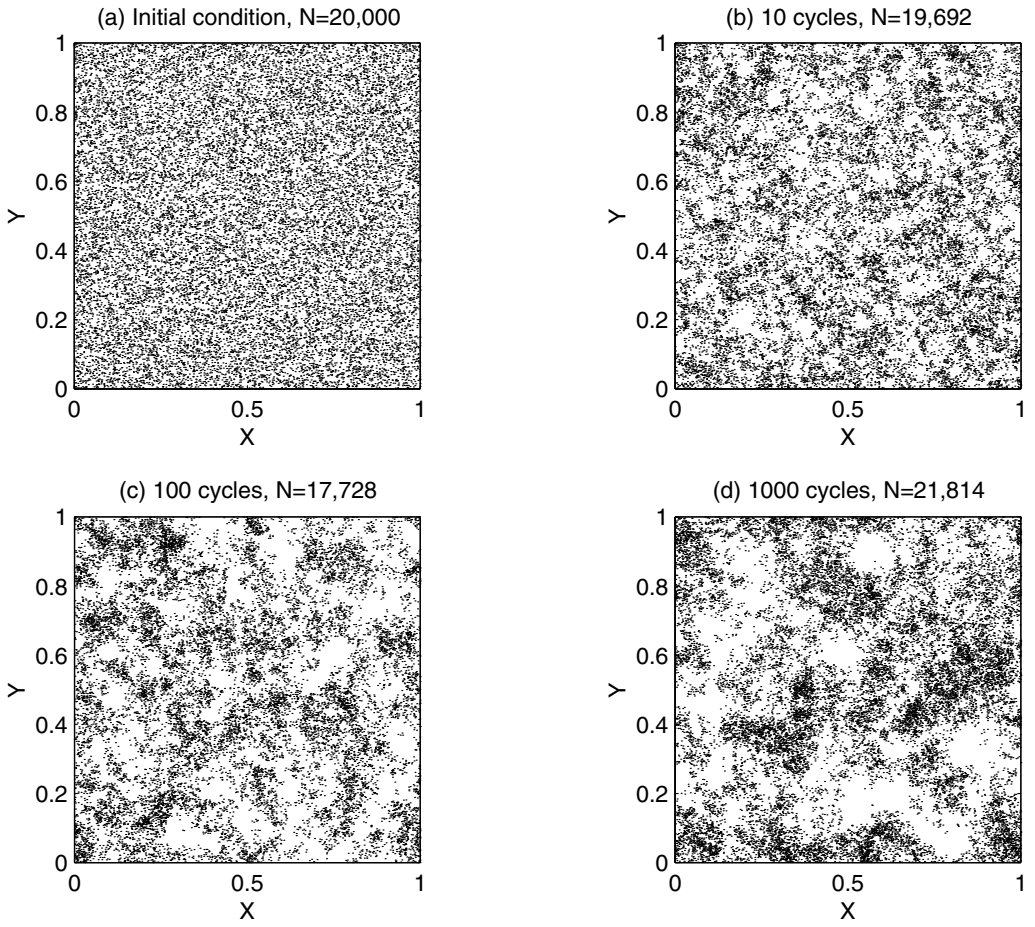

Figure 8: (a) The initial condition is $N = 20,000$ randomly located bugs in the unit square. Panels (b), (c) and (d) then show the development of patches after 10, 100 and 1000 cycles of random displacement followed by random birth/death. As the panel titles indicate, there are random fluctuations in the total size, N, of the population. The RMS step length of the underlying random walk is $\langle \delta x_k^2 \rangle^{1/2} = \langle \delta y_k^2 \rangle^{1/2} = 0.005$.

problems, with reproduction and death, so fundamentally different from the advection-diffusion of chemical tracers? I am not prepared to answer that question in these lectures and I leave further development of this example to the students.

5 Variance budgets

In this section we return to basics and present an alternative view of eddy-diffusivity. The following arguements emphasize the importance of the concentration variance equation.

5.1 The Reynolds' decomposition

We depart from the advection-diffusion equation

$$c_t + \boldsymbol{u}\cdot\nabla c = \kappa\nabla^2 c + s\,, \tag{36}$$

where κ is the molecular diffusivity of c and $\boldsymbol{u}$ is an incompressible ($\nabla\cdot\boldsymbol{u} = 0$) velocity field. Also in (36) we have included a source term, $s(\boldsymbol{x}, t)$, which forces the system.

The velocity $\boldsymbol{u}$ in (36) is a single realization selected from an ensemble of velocity fields. Then we can introduce the "Reynolds' decomposition":

$$c = \langle c\rangle + c'\,, \tag{37}$$

where $\langle\rangle$ is the ensemble average and c' is the fluctuation from $\langle c\rangle$ which arises in a single realization. Taking the ensemble average of (36) gives

$$\langle c\rangle_t + \langle\boldsymbol{u}\rangle\cdot\nabla\langle c\rangle + \nabla\cdot\langle\boldsymbol{u}'c'\rangle = \kappa\nabla^2\langle c\rangle + s\,. \tag{38}$$

(The source s is taken to be deterministic, $\langle s\rangle = s$.)

Subtracting the ensemble average in (38) from (36) gives the fluctuation equation

$$c'_t + \langle\boldsymbol{u}\rangle\cdot\nabla c' + \nabla\cdot[\boldsymbol{u}'c' - \langle\boldsymbol{u}'c'\rangle] - \kappa\nabla^2 c' = -\boldsymbol{u}'\cdot\nabla\langle c\rangle\,. \tag{39}$$

Equation (39) has been organized by taking the source term to the right hand side. Thus we see that advective distortion of the mean gradient, $\nabla\langle c\rangle$, generates the fluctuation c'.

5.2 Consequences of linearity

If $c' = 0$ at $t = 0$ then, because (39) is linear, c' and $\nabla\langle c\rangle$ will be linearly related. It follows that the eddy flux $\langle\boldsymbol{u}'c'\rangle$ will also be linearly related to the mean gradient $\nabla\langle c\rangle$. These simple observations, in alliance with the

scale separation assumption, can be used to extract a surprising amount of information [2].

The scale separation it is plausible that this linear relation between eddy flux and mean gradient can be developed in a series of the form

$$\langle \boldsymbol{u}' c' \rangle_i = -\mathcal{D}^{(1)}_{ij} * \langle c \rangle_{,j} - \mathcal{D}^{(2)}_{ijk} * \nabla \langle c \rangle_{,jk} + \cdots \tag{40}$$

The $*$ in (40) indicates that the product also involves convolutions in time, such as

$$\mathcal{D}^{(1)}_{ij} * \langle c \rangle_{,j} = \int_0^t \mathcal{D}^{(1)}_{ij}(t') \langle c \rangle_{,ij}(t - t') \, \mathrm{d}t' \, . \tag{41}$$

If the mean field is varying slowly over an eddy decorrelation time then the convolution above approximates to

$$\langle \boldsymbol{u}' c' \rangle \approx -\mathcal{D}^{(1)}_{ij} * \langle c \rangle_{,j} \approx -\int_0^\infty \mathcal{D}^{(1)}_{ij}(t') \, \mathrm{d}t' \, \langle c \rangle_{,j}(t) \, . \tag{42}$$

In the simplest cases[3]

$$\int_0^\infty \mathcal{D}^{(1)}_{ij}(t') \, \mathrm{d}t' = D_e \delta_{ij} \, , \tag{43}$$

where D_e is the eddy diffusivity. Using (43) the flux gradient relation is

$$\langle \boldsymbol{u}' c' \rangle - \kappa \nabla \langle c \rangle = -D \nabla \langle c \rangle \, , \qquad D \equiv D_e + \kappa \, , \tag{44}$$

and the evolution of the average concentration is determined by

$$\langle c \rangle_t \approx D \nabla^2 \langle c \rangle + s \, . \tag{45}$$

5.3 The Gx-trick

The tensors $\mathcal{D}^{(n)}(t)$ are determined by the linear operator on the left hand side of (39). Thus, these tensors depend on *(i)* the statistical properties of $\boldsymbol{u}'$; *(ii)* the mean advection $\langle \boldsymbol{u} \rangle$; *(iii)* the molecular diffusion κ. The essential

[3] "Simple" means that the velocity ensemble is isotropic, homogeneous and reflexionally invariant. The last requirement means that the mirror image of a particular realization of $\boldsymbol{u}'$ is just as probable as $\boldsymbol{u}'$. If the ensemble is reflexionally invariant then $\mathcal{D}^{(1)}_{ij}$ is a symmetric tensor. This subtle point will be illustrated later in this lecture series.

point is that these tensors do not depend on $\langle c \rangle$. At least for the first term in the series, $\mathcal{D}_{ij}^{(1)}$, we can exemplify this by noting that there is a special solution of (36) in which $\langle \boldsymbol{u} \rangle = s = 0$ and concentration has the form

$$c = Gx + c' \,. \tag{46}$$

In (46) the mean concentration is simply $\langle c \rangle = Gx$ and the fluctuation c' is determined from a reduced version of (39):

$$c'_t + \boldsymbol{u}' \cdot \nabla c' - \kappa \nabla^2 c' = -Gu' \,. \tag{47}$$

As emphasized above, the advection of the mean gradient appears as a source term for c' on the right hand side of (47). Because (47) is linear, and G is constant, the solution c' will be proportional to the large-scale gradient G and otherwise independent of G.

This Gx-trick enforces the platonic ideal of scale separation between the eddies and the mean field. If the concept of an eddy diffusivity is to have any validity, then it must work in the simplified context of (47). In fact, the Gx-trick is used in doubly-periodic turbulence simulation to calculate eddy diffusivities. In that context, $\boldsymbol{u}' = (u, v)$ and c' are efficiently represented by Fourier series. Then (47) is solved using a spectral code and the eddy flux is estimated by computing the integral

$$\langle \boldsymbol{u}' c' \rangle = A^{-1} \iint \boldsymbol{u}' c' \, \mathrm{d}x \, \mathrm{d}y \,, \tag{48}$$

over the computational domain. (In (48) A is the total area of the domain so $\langle 1 \rangle = 1$). Notice that in (48) the ensemble average is identified with an integral over the domain. Later in these lectures we will use this same procedure to analytically calculate the eddy diffusivities of some spatially periodic velocity fields.

5.4 The concentration variance equation

An equation for the concentration variance,

$$\mathcal{Z} \equiv \frac{1}{2} \langle c'^2 \rangle \,, \tag{49}$$

is obtained by multiplying (39) by c' and ensemble averaging. The result is

$$\mathcal{Z}_t + \langle \boldsymbol{u} \rangle \cdot \nabla \mathcal{Z} + \nabla \cdot \langle \frac{1}{2} \boldsymbol{u}' c'^2 \rangle - \kappa \nabla^2 \mathcal{Z} = -\kappa \langle \nabla c' \cdot \nabla c' \rangle - \langle \boldsymbol{u}' c' \rangle \cdot \nabla \langle c \rangle \,. \tag{50}$$

The terms on the left hand side of (50) can be interpreted as fluxes of $\mathcal{Z}$. The two terms on the right hand side of (57) are respectively a source of variance due to advective distortion of the mean gradient, and dissipation of variance by molecular diffusion κ.

5.5 Heuristic closure arguments

In (50) there are three terms which we would like to relate to the mean quantities $\langle c\rangle$ and $\mathcal{Z}$. First, there is $-\langle \boldsymbol{u}' c'\rangle \cdot \nabla\langle c\rangle = D_e \nabla\langle c\rangle \cdot \nabla\langle c\rangle$. The remaining two terms are $\langle \boldsymbol{u}' c'^2/2\rangle$ and $\kappa\langle \nabla c' \cdot \nabla c'\rangle$.

The correlation $\langle \boldsymbol{u}' c'^2/2\rangle$ in (50) is an eddy-flux of c'^2, just as $\langle \boldsymbol{u} c'\rangle$ is an eddy flux of c'. Thus, by analogy with (44), we can argue that

$$\frac{1}{2}\langle \boldsymbol{u}' c'^2\rangle = -D_e \nabla \mathcal{Z}\,. \tag{51}$$

This heuristic argument is discussed further in appendix B.

The final term in (50) is the dissipation of variance by molecular diffusivity, $\kappa\langle \nabla c' \cdot \nabla c'\rangle$. The simplest closure assumption we can make about this term is that

$$\kappa\langle \nabla c' \cdot \nabla c'\rangle \approx \beta \mathcal{Z}\,, \tag{52}$$

where β has the dimensions of time. The closure above relies on dimensional analysis and the linearity of (36). However, in anticipation of a later discussion of the Batchelor spectrum, we now make some heuristic arguments in support of (52) which suggest that β is independent of the molecular diffusivity.

Suppose that the mean field $\langle c\rangle$ has a length scale L and that the velocity field $\boldsymbol{u}'$ has a length scale $L_{\boldsymbol{u}}$ (in the RW example $L_{\boldsymbol{u}} = k^{-1}$). The scale separation assumption is that

$$L \gg L_{\boldsymbol{u}}\,. \tag{53}$$

The inequality in (53) is exemplified in idealized case of (46) in which L is infinite. If follows that advective distortion of $\nabla\langle c\rangle$ generates c' first on the scale $L_{\boldsymbol{u}}$. Then, following our arguments in lecture 1, the scale of c' will be exponentially reduced, like $\exp(-\gamma t)$, where γ is roughly proportional to the

RMS strain of $\boldsymbol{u}'$. This exponential contraction continues till the *cascade* is halted by molecular diffusion at the scale

$$\ell \equiv \sqrt{\frac{\kappa}{\gamma}}\,. \tag{54}$$

Using arguments from lecture 1, we can estimate that the time taken for this arrest at ℓ is

$$t_\ell \approx \gamma^{-1} \ln\left(L_{\boldsymbol{u}}/\ell\right)\,. \tag{55}$$

Then the smallest length scale in the c'-field is ℓ and, plausibly, the gradient is $\nabla c' \sim c'_{RMS}/\ell$ where $c'_{RMS} \equiv \sqrt{2\mathcal{Z}}$. We now have a simple estimate $\kappa\langle\nabla c'\cdot\nabla c'\rangle \sim \gamma\mathcal{Z}$. This rough argument leads to the closure in (52), with $\beta \propto \gamma$, and the caveat that $t > t_\ell$.

We can summarize the arguments above by rewriting the variance equation (50) as

$$\mathcal{Z}_t + \langle\boldsymbol{u}\rangle\cdot\nabla\mathcal{Z} - D\nabla^2\mathcal{Z} = D_e\nabla\langle c\rangle\cdot\nabla\langle c\rangle - \beta\mathcal{Z}\,, \qquad (\text{if } t \geq t_\ell)\,. \tag{56}$$

The most dubious approximation is probably (52). To conclude this discussion we will interpret the variance equation in two specific examples.

5.6 Example 1: the dispersing front

First consider the dispersing front in figure 5. In this example $s = \kappa = \langle\boldsymbol{u}\rangle = 0$ and we have already know from (28) that

$$\mathcal{Z} = \frac{1}{2}\left[1 - \mathrm{erf}^2\left(\eta\right)\right]\,, \qquad \eta = \frac{x}{2\sqrt{Dt}}\,. \tag{57}$$

On the other hand, since $\kappa = 0$, it follows that $D = D_e$ and $\beta = 0$. With these simplifications the variance equation (50) reduces to

$$\mathcal{Z}_t - D\mathcal{Z}_{xx} = D\nabla\langle c\rangle\cdot\nabla\langle c\rangle\,, \tag{58}$$

where $\langle c\rangle$ is the erf-solution in (25). As a consistency check, one can show that (57) is the solution of the variance equation in (58).

This example shows that the destruction of variance by molecular diffusivity is not required in order to prevent an accumulation of variance: the source on the right hand side of (58) is balanced by eddy diffusion.

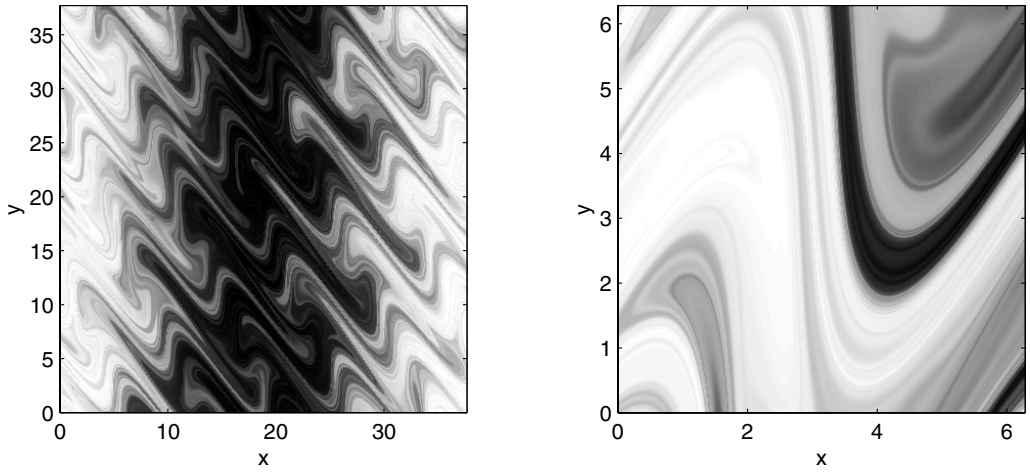

Figure 9: A simulation of the source problem, with $s = \cos(x/6)$, using the RW model to generate $\boldsymbol{u}$ in (36). There is no molecular diffusivity ($\kappa = 0$). The left hand panel shows the whole domain (the length of the side is 12π) while the right hand panel shows a smaller subdomain (the length of the side is 2π). The concentration fields were generated by 10 pulses of the renovating wave using $\tau_* = 3$ (that is, $t = 30$).

5.7 Example 2: a large-scale source

In this second example the tracer is injected by a source $s = \cos qx$ in (36). We also take $\langle \boldsymbol{u} \rangle = 0$ so that the mean concentration field is obtained by solving

$$\langle c \rangle_t - D\nabla^2 \langle c \rangle = \cos qx\,, \quad \Rightarrow \quad \langle c \rangle = \frac{1}{Dq^2}\left[1 - e^{-Dq^2 t}\right] \cos qx\,. \tag{59}$$

(To apply the diffusion equation the scale of the source, q^{-1}, must be much larger than the scale of the velocity field.) A steady mean concentration pattern is established when $Dq^2 t \gg 1$.

The concentration variance is determined by solving the variance equation (56)

$$\mathcal{Z}_t - D\nabla^2 \mathcal{Z} = \frac{1}{2}\frac{D_e}{D^2 q^2}\left[1 - e^{-Dq^2 t}\right]^2 (1 - \cos 2qx) - \kappa \langle \nabla c' \cdot \nabla c' \rangle\,. \tag{60}$$

In (60), the solution in (59) has been used to evaluate the source term on the right hand side and we have left the diffusive sink in its exact form.

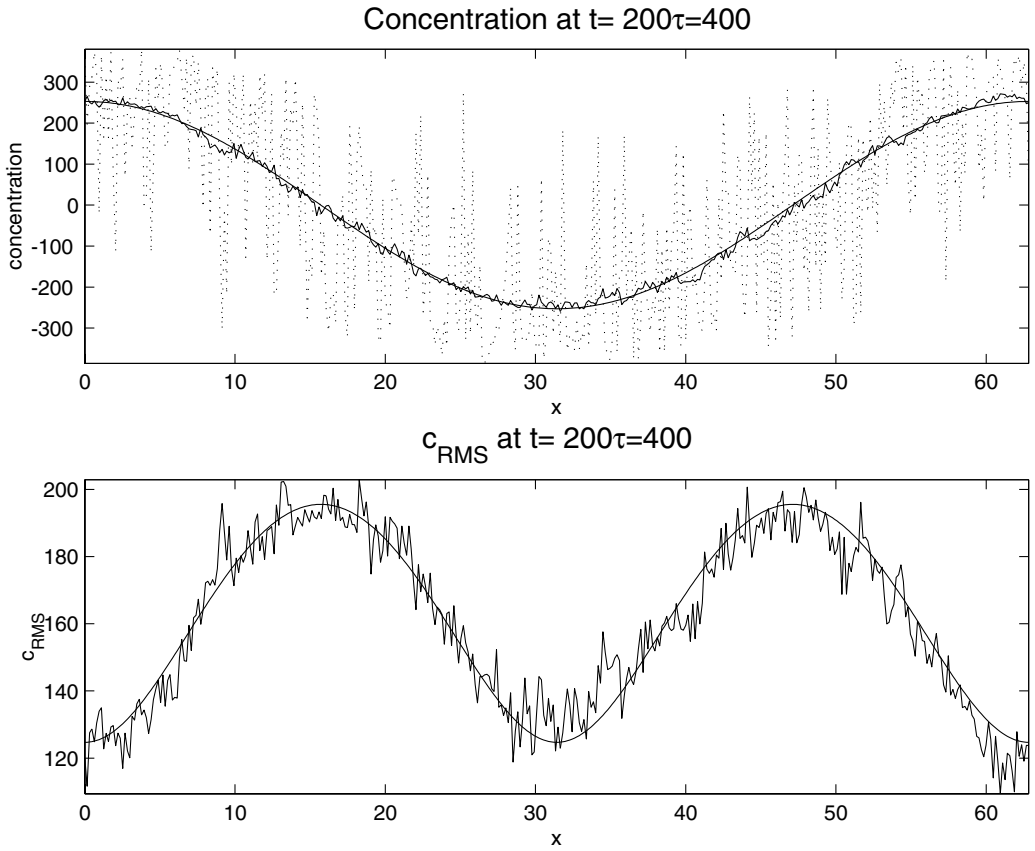

Figure 10: This figure compares analytic results with a numerical solution of (62), taking $q = 1/10$, and using the RW model to generate $\boldsymbol{u}$. The persistence parameter is $\tau_* = 2$ and the results are at $t = 400$ (that is, 200 renovation cycles). The concentration $c(\boldsymbol{x}, 400)$ is calculated on a 400×400 grid using the method in appendix B. In the top panel there are three curves: the concentration as a function of $0 < x < 20\pi$ along the line $y = 0$ (the jagged dotted curve); the y-averaged concentration defined in (64); the analytic result in (59) (the smooth sinusoid). The bottom panel compares the $c_{RMS} = \sqrt{2\mathcal{Z}}$ obtained by solving (60) analytically with c_{RMS} estimated using (64).

It is clear from (60) that the molecular diffusion, κ, plays an important role. If $\kappa = 0$ then the long time solution of (60) has a component which eventually grows linearly with time:

$$\kappa = 0\,, \qquad \Rightarrow \qquad \mathcal{Z} \propto t/2Dq^2\,. \tag{61}$$

Thus, without molecular diffusion, there is "runaway variance". Ultimately, in a single realization, the mean field in (59) will be buried under enormous fluctuations.

To give an intuitive derivation of (61) we argue that with $\kappa = 0$ the concentration on each fluid element is determined by solving the Lagrangian equation

$$\frac{Dc}{Dt} = \cos qx(t)\,, \tag{62}$$

where $x(t)$ is the randomly changing x-position of the particle. Thus, the concentration on each particle is undergoing a random walk along the c-axis, which is induced by the random motion of the particle through the $\cos qx$ source function. The decorrelation time of this walk is the time it takes a particle to diffuse through a distance of order q^{-1}, which is $1/Dq^2$. Thus, in a time t, there are roughly $N(t) \sim Dq^2t$ independent steps along the c-axis. But because the source acts coherently for a time $1/Dq^2$ with a strength of order unity, the step length of this random walk is roughly $\Delta c \sim 1/Dq^2$. Thus, the mean square displacement of c is:

$$\langle c'^2 \rangle \sim (\Delta c)^2 N(t) \sim \frac{t}{Dq^2}\,, \tag{63}$$

which is the final result in (61).

It is interesting to compare the analytic results in (59) and (60) with a numerical solution of (62). Thus we must compute the spatial averages

$$\bar{c}(x,t) \equiv \frac{1}{L}\int_0^L c(x,y,t)\,\mathrm{d}y, \qquad c^2_{RMS}(x,t) \equiv \frac{1}{L}\int_0^L [c(x,y,t)-\bar{c}]^2\,\mathrm{d}y\,, \tag{64}$$

using the numerical solution, and compare these with the analytic results for $\langle c \rangle$ and $\mathcal{Z} = c^2_{RMS}/2$. The best way to make this comparison is to obtain $c(x,y,t)$ on a regular grid in the (x,y)-plane. As a bonus, one can then also use contouring routines to make pretty pictures of the concentration field (see figure 9).

The concentration field is calculated on a regular grid using the procedure described in Appendix C (essentially the method of characteristics). Figure 10 shows good agreement between this simulation and analytic results. Notice that in figure 10 the variance $\mathcal{Z}$ peaks where $\nabla\langle c \rangle$ is greatest. This illustrates that concentration fluctuations are produced by advective

distortion of the mean gradient: where the mean gradient is large there is lots of variance. But $\mathcal{Z} \neq 0$ even where $\nabla\langle c\rangle = 0$ (for example, at $x = 0$ and $x = 10\pi$ in figure 10). Thus, where the source term on the right hand side of (60) vanishes, the diffusive term $D\nabla^2\mathcal{Z}$ supplies variance.

5.8 Cautionary remarks

In the both examples above there is no molecular diffusion ($\kappa = 0$) and consequently there is no destruction of variance by the term $\kappa\langle\nabla c'\cdot\nabla c'\rangle$ in (50). As a project for a student, include molecular diffusion in the RW model (perhaps by pulsing diffusion in alternation with advection) and assess the efficacy of this process. In particular, can the closure in (52) be justified?

6 Calculation of the RW Green's function

In this appendix we present an alternative calculation of the RW ensemble averaged Green's function, $g(r)$, in (17). The unaveraged Green's function, $G(\boldsymbol{x}, \boldsymbol{x}_0, t)$, is the solution of (10). Because the process is spatially homogeneous it is harmless to take $\boldsymbol{x}_0 = 0$ so that

$$G(\boldsymbol{x}, 0, \tau_*) = \delta\left[x - \tau_* s\sin\varphi\right]\delta\left[y + \tau_* c\sin\varphi\right]\,, \tag{65}$$

where $(s, c) \equiv (\sin\theta, \cos\theta)$. The ensemble average of (65) is computed by integration over φ and θ, as in (4). It is very pleasant that there are two integrals and two δ-functions. Thus, we first do the φ-integral by noting that $\delta\left[x - \tau_* s\sin\varphi\right]$ is nonzero at the two values of φ where $\sin\varphi = x/\tau_* s$, and at those positions:

$$\frac{\mathrm{d}}{\mathrm{d}\varphi}\left[x - \tau_* s\sin\varphi\right] = \pm\sqrt{\tau_*^2 s^2 - x^2}\,. \tag{66}$$

Using the standard rule for changing variables in a δ-function, we find that the average of (65) over φ alone is

$$\langle G\rangle_\varphi = \frac{1}{\pi}\frac{\delta(y + \cot\theta x)}{\sqrt{\tau_*^2\sin^2\theta - x^2}}\,. \tag{67}$$

The second integral over θ is performed by noting that $\delta(y+\cot\theta x)$ is nonzero at the two values of θ where $\cot\theta = -y/x$, and at those positions

$$\sin^2\theta = \frac{x^2}{x^2 + y^2}\,, \qquad \frac{\mathrm{d}}{\mathrm{d}\theta}\left[y + x\cot\theta\right] = -\frac{x^2 + y^2}{x}\,. \tag{68}$$

After changing variables in the δ-function we recover $g(r)$ in (17).

7 Eddy diffusion of variance

Ignoring small molecular diffusion ($\kappa = 0$), if c satisfies the advection equation then any function of c satisfies the same equation. That is to say

$$\frac{Dc}{Dt} = 0, \qquad \Rightarrow \qquad \frac{Df}{Dt} = 0\,, \tag{69}$$

where $f(c) = c^2$, or $\exp(c)$ etcetera. Taking an ensemble average, and making the same arguments for $f(c)$ as for c, we have that

$$\langle f\rangle_t = D\nabla^2\langle f\rangle\,. \tag{70}$$

In the particular case $f = c^2/2$, $\langle f\rangle = \langle c\rangle^2/2 + \mathcal{Z}$ and (70) reduces to

$$\mathcal{Z}_t = D\nabla^2\mathcal{Z} + D\nabla\langle c\rangle\cdot\nabla\langle c\rangle\,. \tag{71}$$

Matching the terms in (71) with those in (50) we conclude that $\langle \boldsymbol{u}'{c'}^2/2\rangle = -D\nabla\mathcal{Z}$.

8 Numerical simulation of the RW process

Drawing figures 9 and 10 requires that we obtain the solution of (62) on a regular grid in the (x, y)-plane. This is an opportunity to use the method of characteristics and learn some MATLAB programming techniques.

Equation (3) shows how the movement of a particle in the RW velocity field is equivalent to a random map which determines the position at $(n+1)\tau_*$ in terms of the previous position at $n\tau_*$. If this particle carries a concentration, $c(\boldsymbol{x}, t)$, which changes because of the $\cos qx$ source in (62), then the concentration changes can also be calculated and expressed as a map in discrete time.

Thus, suppose that the concentration on a particle at time $t = n\tau_*$ is c_n. Then the change in concentration during $n\tau_* < t < (n+1)\tau_*$ is obtained by integrating

$$\frac{Dc}{Dt} = \cos\left[qx_n + qu_n(t - n\tau_*)\right]\,, \tag{72}$$

where the x-velocity of the particle is $u_n = s_n \sin(c_n x_n + s_n y_n + \varphi_n)$, with $(s_n, c_n) \equiv (\sin\theta_n, \cos\theta_n)$ is the constant velocity of the particle. The integral of (72) can be written as

$$c_{n+1} = c_n + \frac{\sin(qx_{n+1}) - \sin(qx_n)}{qu_n}\,. \tag{73}$$

With equations (73) and (3) we can integrate forward in time and so determine the concentration on a particle at $t = n\tau_*$.

However we need to determine the concetration at $t = n\tau_*$ at a specified grid point $\boldsymbol{x}$. So the trick is to...

```
%% Solution of
%%
%%   Dc/Dt=cos(qx);
%%
%%  cos(q x) is a large -scale source and u is the RW velocity.
%%  The RW streamfunction is psi=cos[cos(theta) x+ sin(theta)y + phi]
clc
N=400;              %% Use an N*N grid in the plotting window
q=1/6;              %% The wavenumber of the cos q x source
LL=2*pi/q;          %% LL is the domain size
npulse=10           %% The number of renovation cycles
tau=3;              %% The pulse duration of the wave

%% Lwin is the side of the square plotting window.
%% Set Lwin=LL to see the big picture. To see small scale details,
%% try Lwin = 2*pi. We draw two subplots with different Lwin's
nloop=0;
 for Lwin=[LL 2*pi]
   nloop=nloop+1
       x=linspace(0,Lwin,N);   %% x is the coordiante in the plotting window.
       h=x(2);                 %% The grid spacing in the plotting window

         for j=1:N
          jj=[((j-1)*N+1):(j*N)];
          pos(jj,1)=zeros(N,1)+(j-1)*h;
          pos(jj,2)=x';
```

```
        end

      conc=zeros(N*N,1);

  %% The position of the N^2 particles are stored in pos with
  %% N^2 rows and 2 columns. Each vertical segment of
  %% length N in pos contains particles with the same initial x-position.
  %% the column vector conc contains the concentration on the
  %% N*N particles in pos. Initially, conc=0 at the N*N
  %%  grid points. Then we integrate
  %% backwards in time to find the concentration change.

     for k=1:1:npulse
       theta=rand*2*pi;
       wavevec=[cos(theta),sin(theta)]';
           phase=rand*2*pi;
       vel=sin(pos*wavevec+phase)*[wavevec(2),-wavevec(1)];
       conc=conc-sin(q*pos(:,1))./(q*vel(:,1));
       pos=pos+tau*vel;
       conc=conc +sin(q*pos(:,1))./(q*vel(:,1));
     end

%% Emerging from this loop, we have the the new positions
%% and the new concentration

  conc=reshape(conc,N,N); %% conc is reshaped into an N*N matrix
  hh=subplot(1,2,nloop)
  colormap('gray')
  imagesc(x,x,conc)
  axis equal
  xlabel('x')
  ylabel('y')
  axis([0 Lwin 0 Lwin])
  set(hh,'ydir','norm')

end
```

References

[1] S. Childress and A. D. Gilbert. *Stretch, Twist, Fold: The Fast Dynamo*. Springer, Berlin, 1995.

[2] H.K.Moffatt. Transport effects associated with turbulence with particular attention to the influence of helicity. *Rep. Prog. Phys.*, 46:621–664, 1983.

[3] W.A. Medeiros. *Marbling Techniques*. Watson-Guptill, New York, 1994.

[4] G.I. Taylor. Eddy motion in the atmosphere. *Phil. Trans. Roy. Soc. London*, 215:1–16, 1915.